




Impact of functional studies on exome sequence variant interpretation in early-onset cardiac conduction system diseases

Kenshi Hayashi ^{1*}†, Ryota Teramoto ^{1,2†}, Akihiro Nomura ¹, Yoshihiro Asano ³,
Manu Beerens ², Yasutaka Kurata⁴, Isao Kobayashi⁵, Noboru Fujino¹,
Hiroshi Furusho ¹, Kenji Sakata¹, Kenji Onoue⁶, David Y. Chiang ²,
Tuomas O. Kiviniemi ², Eva Buys², Patrick Sips ^{2,7}, Micah L. Burch ²,
Yanbin Zhao², Amy E. Kelly², Masanobu Namura⁸, Yoshihito Kita⁹,
Taketsugu Tsuchiya ¹⁰, Bunji Kaku¹¹, Kotaro Oe ¹², Yuko Takeda¹, Tetsuo Konno¹,
Masaru Inoue¹³, Takashi Fujita¹⁴, Takeshi Kato ¹, Akira Funada¹, Hayato Tada¹,
Akihiko Hodatsu¹, Chiaki Nakanishi¹, Yuichiro Sakamoto¹⁵, Toyonobu Tsuda¹,
Yoji Nagata¹, Yoshihiro Tanaka¹, Hirofumi Okada¹, Keisuke Usuda ¹, Shihe Cui¹,
Yoshihiko Saito⁶, Calum A. MacRae ², Seiji Takashima¹⁶, Masakazu Yamagishi^{1,17},
Masa-aki Kawashiri¹, and Masayuki Takamura ¹

¹Department of Cardiovascular Medicine, Kanazawa University Graduate School of Medical Sciences, 13-1, Takara-machi, Kanazawa, Ishikawa 920-8641, Japan; ²Division of Cardiovascular Medicine, Department of Medicine, Brigham and Women's Hospital and Harvard Medical School, Boston, MA, USA; ³Department of Cardiovascular Medicine, Osaka University Graduate School of Medicine, Suita, Japan; ⁴Department of Physiology, Kanazawa Medical University, Uchinada, Japan; ⁵Faculty of Biological Science and Technology, Institute of Science and Engineering, Kanazawa University, Kanazawa, Japan; ⁶Cardiovascular Medicine, Nara Medical University, Kashihara, Japan; ⁷Center for Medical Genetics Ghent, Department of Biomolecular Medicine, Ghent University, Ghent, Belgium; ⁸Department of Cardiology, Kanazawa Cardiovascular Hospital, Kanazawa, Japan; ⁹Department of Internal Medicine, Wajima Municipal Hospital, Wajima, Japan; ¹⁰Trans-catheter Cardiovascular Therapeutics, Kanazawa Medical University, Uchinada, Japan; ¹¹Division of Cardiovascular Medicine, Toyama Red Cross Hospital, Toyama, Japan; ¹²Division of Internal Medicine, Saiseikai Kanazawa Hospital, Kanazawa, Japan; ¹³Department of Cardiology, Ishikawa Prefectural Central Hospital, Kanazawa, Japan; ¹⁴Division of Cardiology, Kouseiren Takaoka Hospital, Takaoka, Japan; ¹⁵Division of Cardiology, Toyohashi Heart Center, Toyohashi, Japan; ¹⁶Department of Medical Biochemistry, Osaka University Graduate School of Medicine, Suita, Japan; and ¹⁷Osaka University of Human Sciences, Settu, Japan

Received 22 March 2019; revised 2 October 2019; editorial decision 30 December 2019; accepted 17 January 2020; online publish-ahead-of-print 24 January 2020

Time for primary review: 40 days

Aims

The genetic cause of cardiac conduction system disease (CCSD) has not been fully elucidated. Whole-exome sequencing (WES) can detect various genetic variants; however, the identification of pathogenic variants remains a challenge. We aimed to identify pathogenic or likely pathogenic variants in CCSD patients by using WES and 2015 American College of Medical Genetics and Genomics (ACMG) standards and guidelines as well as evaluating the usefulness of functional studies for determining them.

Methods and results

We performed WES of 23 probands diagnosed with early-onset (<65 years) CCSD and analysed 117 genes linked to arrhythmogenic diseases or cardiomyopathies. We focused on rare variants (minor allele frequency < 0.1%) that were absent from population databases. Five probands had protein truncating variants in *EMD* and *LMNA* which were classified as 'pathogenic' by 2015 ACMG standards and guidelines. To evaluate the functional changes brought about by these variants, we generated a knock-out zebrafish with CRISPR-mediated insertions or deletions of the *EMD* or *LMNA* homologs in zebrafish. The mean heart rate and conduction velocities in the CRISPR/Cas9-injected embryos and F2 generation embryos with homozygous deletions were significantly decreased. Twenty-one variants of uncertain significance were identified in 11 probands. Cellular electrophysiological study and *in vivo* zebrafish cardiac assay showed that two variants in *KCNH2* and *SCN5A*, four variants in *SCN10A*, and one variant in *MYH6*

* Corresponding author. Tel: +81 76 265 2254; fax: +81 76 234 4251, E-mail: kenshi@med.kanazawa-u.ac.jp

† The first two authors contributed equally to this work.

damaged each gene, which resulted in the change of the clinical significance of them from 'Uncertain significance' to 'Likely pathogenic' in six probands.

Conclusion

Of 23 CCSD probands, we successfully identified pathogenic or likely pathogenic variants in 11 probands (48%). Functional analyses of a cellular electrophysiological study and *in vivo* zebrafish cardiac assay might be useful for determining the pathogenicity of rare variants in patients with CCSD. *SCN10A* may be one of the major genes responsible for CCSD.

Keywords

Cardiac conduction system disease • Whole exome sequencing • 2015 ACMG standards and guidelines • CRISPR/Cas9-mediated gene knock-out in zebrafish • Cellular electrophysiological study

1. Introduction

Bradyarrhythmia is a common clinical finding and can be usually due to a physiologic reaction, pharmacotherapy, or advanced age. Patients with bradyarrhythmia may present with syncope, symptoms of heart failure, and rarely sudden cardiac death. The cardiac conduction system consists of the sinus node, atrioventricular (AV) node, and His-Purkinje system. Bradyarrhythmia can be categorized on the level of disturbances in the hierarchy of this system and includes sinus node dysfunction and AV conduction disturbances or blocks.¹

The pathophysiologic mechanisms underlying cardiac conduction system disease (CCSD) are divided into acquired or inherited causes. Several studies showed genetic variants associated with CCSD linked to either structurally normal heart diseases or structural heart diseases.¹⁻³ Thus, high-throughput sequencing (HTS) may be helpful in determining the causes of CCSD because of their comprehensiveness.⁴ Advancement of HTS has identified lots of putative variants associated with inherited cardiac disease. However, determining true pathogenicity of targeted diseases is still a major challenge.⁵

In 2015, the American College of Medical Genetics and Genomics (ACMG), the Association for Molecular Pathology (AMP), and the College of American Pathologists reported updated standards and guidelines for the classification of sequence variants using criteria informed by expert opinion and empirical data.⁶ This guideline is useful for the consistent and reliable interpretation of genetic variants, but it also identifies many variants of uncertain significance, which are of limited use in medical decision-making.

Of these criteria, functional studies could be one of the powerful tools in support for disease pathogenicity.⁶ The gold standard for the functional analysis of ion channel variants is an electrophysiological measurement using a patch-clamp method in cell expression systems and a simulation study with mathematical models of human cardiomyocytes.⁷ Zebrafish is an emerging model for studying cardiac diseases, including cardiac arrhythmia, and for determining the pathogenicity of unknown genes detected by whole-exome sequencing (WES) or HTS.^{8,9} The recent sequencing of zebrafish has revealed that approximately 70% of human genes have functional homologs in zebrafish.¹⁰ Moreover, CRISPR/Cas9-mediated gene knock-out in zebrafish can facilitate high-throughput screens for phenotypic effects with high levels of on-target efficiency and relatively off-target modifications.^{11,12} However, *in vivo* zebrafish cardiac assay using CRISPR/Cas9 systems has not been fully established for interpreting pathogenicity of human rare variants associated with CCSD.

Here, we assessed 23 probands diagnosed with early-onset CCSD with pacemaker implantation (PMI) or a family history of PMI. We used a prioritization approach with 117 arrhythmia and cardiomyopathy-

related genes in conjunction with WES for these patients, and classified the variants according to the ACMG standards and guidelines. Then, we performed functional studies to re-classify guideline-based pathogenicity for these variants, using a patch-clamp method in heterologous expression systems and a simulation study for ion channel variants, and *in vivo* zebrafish cardiac assay for non-ion channel variants.

2. Methods

All data and supporting materials have been provided in the published article. An expanded Methods section is available in the [Supplementary material online](#).

2.1 Study patients

The study conformed with the principles outlined in the Declaration of Helsinki and was approved by the Ethics Committee for Medical Research at our institution. All study patients provided written informed consent before registration.

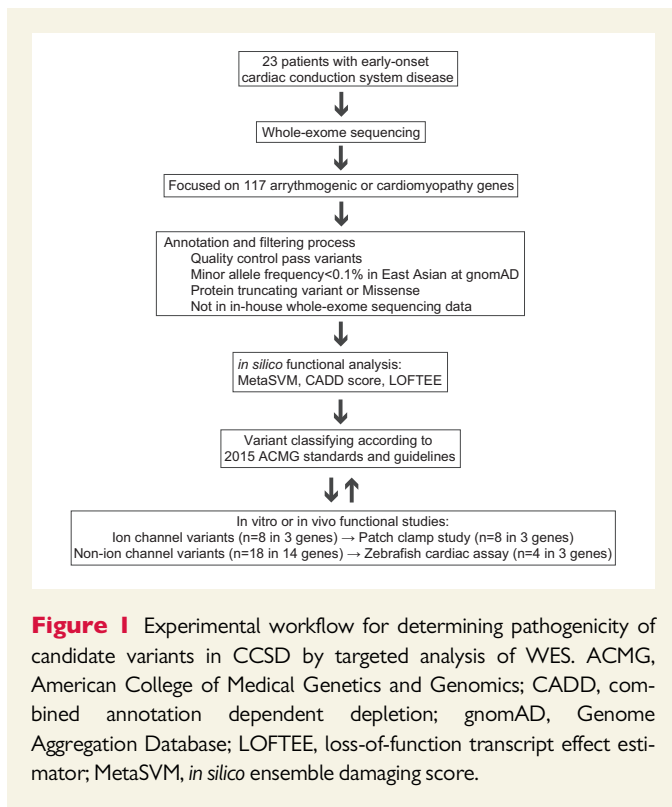
The study patients were recruited from multiple hospitals in Japan. Early-onset CCSD was defined as bradyarrhythmia occurring in individuals aged <65 years, who showed an AV block and/or a sick sinus syndrome (SSS) with PMI or a family history of PMI. In addition, we used DNA-sequencing data of 102 control subjects without electrocardiogram (ECG) abnormality.

2.2 WES and determining pathogenicity of candidate variants

WES was performed using the Illumina HiSeq (Illumina, San Diego, CA, USA). We extracted variants from 117 candidate genes linked to monogenic arrhythmogenic disorders or cardiomyopathies ([Supplementary material online, Table S1](#)) and conducted standard quality control analysis. All variants were annotated by the Variant Effect Predictor version 82 and referred following *in silico* damaging scores: MetaSVM for missense variants; LOFTEE for protein truncating variants (PTVs); and CADD for all variants.¹³ Then, we interpreted these annotated variants using 2015 ACMG standards and guidelines, which provided criteria for the classification of pathogenic or likely pathogenic variants ([Figure 1](#)).⁶ These variants were retained if they were found in the database of arrhythmia cases in Osaka University and Nara Medical University.

2.3 *In vivo* zebrafish cardiac assay

All zebrafish experiments have been approved by Institutional Animal Care and Use Committee, which is certified by the Association for Assessment and Accreditation of Laboratory Animal Care, and the Bioethical Committee on Medical Research, School of Medicine,



Kanazawa University. The procedures were also performed in compliance with the National Institutes of Health (NIH) Guide for the Care and Use of Laboratory Animals. Zebrafish euthanasia was performed following NIH and American Veterinary Medical Association guidelines using an overdose of Tricaine in combination with hypothermic shock.

The gene editing in zebrafish with CRISPR/Cas9 was conducted to evaluate detected PTV in *LMNA* or *EMD* from a patient with early-onset CCSB. Cardiac phenotypes were scored at 48 and 72 h post-fertilization (hpf), and genomic DNA was prepared from individuals for Sanger sequencing. The heart rate (HR) was visually counted at 48 hpf by using a stereomicroscope. Cardiac function was evaluated at 48 hpf by using video microscopy with upright microscope. Voltage mapping was recorded on isolated 72 hpf zebrafish hearts.¹⁴ Luciferase units were measured in CRISPR/Cas9 injected *nppb*: F-Luc zebrafish embryos at 5 days of post-fertilization to evaluate the expression levels of the cardiac natriuretic peptide B.¹⁵

With respect to mosaic founders (F0) with *lmna* knockout, they were raised and were outcrossed to a wild-type (WT) line at the age of 3 months (Supplementary material online, Figure S1). Heterozygous F1 fishes with same *lmna* mutation were incrossed, and cardiac phenotypes for F2 embryos were evaluated as described above. Each F2 embryo was genotyped after evaluation of the cardiac phenotype to distinguish between heterozygous and homozygous carriers. Nuclear structure of cardiomyocytes in WT *lmna*^{+/+} and homozygous *lmna*^{del/del} adult zebrafish was evaluated using immunohistochemistry and confocal microscopy. The expression levels of *nppb* gene in *lmna*^{+/+} and *lmna*^{del/del} adult zebrafish were tested using reverse transcription and quantitative PCR.

To generate mutant lines for evaluating the F0 generation, we also used a rapid knockout method, known as acute CRISPR (aCRISPR).¹⁶ Four guide RNAs synthesized from crRNA and tracrRNA and Cas9 protein were co-injected into 1-cell stage cells, whereas the tracrRNA and Cas9 mix was injected in cells from the same clutch as controls.

To characterize a human *MYH6* variant, a *myh6* ATG-blocking morpholino antisense oligonucleotide (*myh6* ATG-MO) (1 ng/embryo) was injected alone or co-injected with human WT or mutant *MYH6* cRNA (0.4 ng/embryo) at the 1- to 2-cell stage, as described previously.¹⁷ The HR and cardiac function were evaluated at 48 hpf. Voltage mapping was recorded on isolated 72 hpf zebrafish hearts.

2.4 Plasmid constructs and electrophysiology

Mutant cDNAs were constructed by an overlap extension strategy or using a QuikChange XL Site-Directed Mutagenesis Kit (Agilent Technologies, Santa Clara, CA, USA). Mammalian cells were transfected with the cDNA encoding potassium or sodium channels and green fluorescent protein (GFP). Cells displaying green fluorescence 48–72 h after transfection were subjected to electrophysiological analysis. Rapidly activating delayed-rectifier potassium current (I_{Kr}) and fast sodium current (I_{Na}) were measured using the whole-cell patch clamp technique with an amplifier, Axopatch-200B (Molecular Devices, Sunnyvale, CA, USA), at room temperature.

2.5 Simulations of cardiac action potentials

With mathematical models of human ventricular myocytes¹⁸ and rabbit peripheral sinoatrial node (SAN) cells,¹⁹ we evaluated effects of the mutational changes in kinetic behaviour of I_{Kr} and I_{Na} on the mid-myocardial action potential configuration of the ventricular myocyte model and pacemaker activity of the peripheral SAN cell model connected to the atrial membrane model via the gap junction conductance. Dynamic behaviours of the model cell were determined by solving a system of non-linear ordinary differential equations numerically. Detailed procedures for simulations are described in the previous articles.^{18,19}

2.6 Statistical analysis

Pooled electrophysiological data were expressed as mean \pm standard error. Two-tailed Student's *t*-test was used for the single comparisons between the two groups. One-way analysis of variance, followed by a Bonferroni *post hoc* test, was used to analyse data with equal variance among three or more groups. A $P < 0.05$ was considered statistically significant. Statistical analysis was performed using JMP Pro 11.0.0 (SAS Institute Inc., NC, USA) and Origin 2018 (OriginLab, Northampton, MA, USA).

3. Results

3.1 Clinical characteristics and molecular genetic analysis of the study cohort

The mean age of the study participants was 40 ± 16 years at the diagnosis of CCSB (Table 1). Of 23 subjects, 12 (52%) were women, 13 (57%) had SSS, 17 (74%) had AV block, and 18 (78%) underwent PMI. Thirteen (57%) had a first-degree family history of PMI. Echocardiographic data revealed a normal mean ejection fraction. Atrial fibrillation (AF) and muscular disease were complicated in 12 (52%) and 2 (10%) subjects, respectively.

Gene analysis showed that five PTVs were identified in *EMD* and *LMNA* where loss of function is a known pathogenicity for CCSB (Table 2). These PTVs were absent from the controls in gnomAD or HGVD. Both CADD and LOFTEE indicated a deleterious effect of these PTVs on each gene (Supplementary material online, Table S2).

Table 1 Clinical characteristics of patients with early-onset cardiac conduction system diseases

Number of probands	23
Female (%)	12 (52)
Age at diagnosis (years)	40 ± 16
Heart rate (b.p.m.)	44 ± 12
Sick sinus syndrome (%)	13 (57)
R-S I/R-S II/R-S III	4/7/2
Atrioventricular block (%)	17 (74)
I/II/III	2/5/10
Family history of PMI	13 (57)
PMI (%)	18 (78)
Atrial fibrillation	12 (52)
LVEF (%)	66 ± 10
Muscular dystrophy	2 (10)

LVEF, left ventricular ejection fraction; PMI, pacemaker implantation; R-S, Rubenstein.

ClinVar or HGMD classified *EMD* p. W226X, *LMNA* c. 1489-2A>G, and *LMNA* p. R321X into pathogenic or disease causing variants. In addition to these 5 PTVs, 1 PTV and 14 missense variants were absent from the controls, 1 PTV and 20 missense variants were considered as deleterious by *in silico* predictive algorithms, and 2 missense variants were classified as disease causing variants by HGMD (Table 2 and Supplementary material online, Table S2). *RBM20* p.1217R was found in a male patient diagnosed with right bundle branch block (RBBB) at age 40 years and complete AV block at age 55 years in Nara Medical University. His younger brother was also diagnosed as RBBB and his grandfather died suddenly in his 70's.

3.2 Clinical characteristics of patients with PTVs in *EMD* or *LMNA*

We identified two PTVs in *EMD* and three PTVs in *LMNA* (Table 2). Two patients harbouring PTVs in *EMD* were diagnosed with CCSD at the age of 33 and 17 years, respectively. They showed AV block and AF in addition to muscular dystrophy, and underwent PMI (Table 3).²⁰ With regard to Patient 1 with *EMD* p. W226X, we previously reported an Emery–Dreifuss muscular dystrophy (EDMD) family including 16 carriers (7 men and 9 women) with *EMD* p. W226X. EDMD caused by *EMD* mutation is associated with X-linked recessive inheritance. All of the seven male carriers had cardiac involvement, and their first cardiac manifestation occurred at age 10–37 years (mean age, 20.9 years).²⁰ In Patient 2, the segregation variant was confirmed in *EMD* (p. Q222X) (Figure 2). Proband's parents did not have this variant which was classified as *de novo* mutation.

Three patients harbouring PTVs in *LMNA* were diagnosed with CCSD at the age of 39, 23, and 44 years, respectively. Patient 3 with *LMNA* K114XfsX1 was a 55-year-old woman (Table 3 and Figure 2). Her ECG showed first-degree AV block at age 39 years and sinus arrest at age 41 years. She had a family history of SCD and PMI. She received PMI at age 42 years and developed AF at 47 years. Echocardiogram showed low normal left ventricular (LV) systolic function. Patient 4 with *LMNA* 1489-2A>G was a 23-year-old man (Table 3 and Figure 2). His mother died suddenly due to ventricular fibrillation at the age of 50 years. His ECG showed AF and complete AV block, and received ICD therapy. Echocardiogram showed normal LV systolic function. Patient 5 with *LMNA* R321X was a 44-year-old woman (Table 3 and Figure 2). She had a

family history of SCD and PMI. Her ECG showed paroxysmal AF at age 32 years and first-degree AV block at age 43 years. She received ICD therapy at the age of 44 years old. Echocardiogram showed normal LV systolic function.

PTVs in *EMD* and *LMNA* could be defined as pathogenic on the basis of '1 very strong (PVS1) and 1 Moderate (PM2) and 1 supporting by the guideline (PP1, PP3, PP4, or PP5)' (Table 2).

3.3 Functional studies of PTVs in *LMNA* and *EMD* using zebrafish

We studied the usefulness of *in vivo* zebrafish assay using CRISPR/Cas9-mediated gene knock-out for interpreting PTVs associated with CCSD. At first, we evaluated the functional effect of one of PTVs, c. 339dupT, p. K114XfsX1 in *LMNA*. We confirmed that the human *LMNA* homolog, *lmna* (ENSDART0000191716.1), in zebrafish was present in only one copy and shared 66% identity with human *LMNA*. The target site was selected around the equivalent *lmna* site of the human *LMNA* c.339dupT (Figure 3A). At 48 hpf after the microinjection of only sgRNA or sgRNA and Cas9 protein, the appearance and the heart morphology of both embryos looked similar (Supplementary material online, Figure S2A). Genomic DNA was prepared from 10 individuals, and Sanger sequencing showed a variety of mutations in sgRNA+Cas9 injected embryos (Supplementary material online, Figure S2A). The mean HR of the sgRNA+Cas9 injected embryos at 48 hpf significantly decreased compared with those of sgRNA injected or non-injected embryos (Supplementary material online, Figure S2B). Voltage mapping on isolated 72 hpf zebrafish hearts showed that the mean conduction velocities of the ventricle (mm/s) were significantly decreased in the sgRNA+Cas9 injected embryos compared with sgRNA injected embryos (8.0 ± 1.2 vs. 16.8 ± 2.6; *P* < 0.01) (Supplementary material online, Figure S2C).

We also evaluated F2 zebrafish embryos. Sequencing analysis of F1 fish after outcross between mosaic founders (F0) and WT fishes showed various truncating indels. Of 10 genotyped F1 fishes, 6 had heterozygous *lmna* c. 319_322 del CGTG, p. E108TfsX5, which caused a premature stop codon (1 male and 5 females) (Supplementary material online, Figure S3). The guide RNA design checker revealed a potential off-target site in *herc1*, to which 2 mismatches in the gRNA design were compared (Supplementary material online, Figure S4A). No mutation was found in the potential off-target site of the 10 genotyped F1 fishes (Supplementary material online, Figure S4B). The appearance and the heart morphology of both F2 embryos looked similar (Figure 3B). The mean HR of *lmna*^{del/del} significantly decreased compared with those of *lmna*^{+/+} (Figure 3C). The evaluation of cardiac function using video microscopy showed that the mean stroke volume, mean cardiac output, and the mean fractional area change of *lmna*^{del/del} significantly increased compared with those of *lmna*^{+/+} (Table 4 and Figure 3D). Voltage mapping on isolated 72 hpf zebrafish hearts showed that mean conduction velocities of both AV canal and ventricle were significantly decreased in *lmna*^{del/del} compared with *lmna*^{+/+} (Table 4 and Figure 3F). Immunostaining analyses demonstrated that both atrial and ventricular cardiomyocytes of *lmna*^{del/del} displayed abnormal nuclear structures compared with those of *lmna*^{+/+} (Supplementary material online, Figure S5A). The mRNA expression levels of *nppb* gene were significantly higher in *lmna*^{del/del} compared with *lmna*^{+/+} (Supplementary material online, Figure S5B).

We also confirmed the functional effect of another PTV, c. 961C>T, p. R321X in *LMNA* using the aCRISPR method for directed knockdown

Table 2 Pathogenic or likely pathogenic variants determined by 2015 ACMG standards and guidelines

Gene	Base change	Amino acid change	PVS1	PS2	PS3	PM2	PP1	PP3	PP4	PP5	BS3	Classification without PS3 (functional studies)	Classification with PS3 (functional studies)	Patient number
EMD	677G>A	W226X	✓		✓	✓	✓	✓	✓	✓		Pathogenic	Pathogenic	1
	664C>T	Q222X	✓	✓	✓	✓		✓				Pathogenic	Pathogenic	2
LMNA	339dupT	K114XfsX1	✓		✓	✓		✓	✓			Pathogenic	Pathogenic	3
	1489-2A>G		✓			✓		✓	✓	✓		Pathogenic	Pathogenic	4
	961C>T	R321X	✓		✓	✓		✓	✓	✓		Pathogenic	Pathogenic	5
KCNH2	805C>T	R269W			✓	✓		✓	✓	✓		Uncertain significance	Likely pathogenic	7
SCN5A	5470C>G	P1824A			✓	✓		✓	✓	✓		Uncertain significance	Likely pathogenic	7
SCN10A	3787C>T	R1263X			✓	✓		✓				Uncertain significance	Likely pathogenic	6
	4444A>G	I1482V			✓	✓	✓	✓	✓			Uncertain significance	Likely pathogenic	8
	5455G>T	D1819Y				✓		✓		✓		Uncertain significance	Uncertain significance	9
	4118T>G	M1373R			✓	✓		✓				Uncertain significance	Likely pathogenic	9
	1519T>C	F507L				✓		✓		✓		Uncertain significance	Uncertain significance	10
	2413G>A	G805S			✓	✓		✓				Uncertain significance	Likely pathogenic	10
MYH6	3347G>A	R1116H				✓		✓	✓			Uncertain significance	Uncertain significance	11
	3755G>A	R1252Q			✓			✓	✓			Uncertain significance	Likely pathogenic	11
RYR2	2300C>G	S767W						✓	✓			Uncertain significance	Uncertain significance	12
MYH7	968T>C	I323T				✓		✓				Uncertain significance	Uncertain significance	10
MYH11	4532G>A	R1511Q				✓		✓	✓			Uncertain significance	Uncertain significance	3
RBM20	3649G>A	G1217R					✓	✓	✓			Uncertain significance	Uncertain significance	6
TTN	70264G>C	G23422R						✓	✓			Uncertain significance	Uncertain significance	14
DES	556G>A	D186N				✓		✓	✓			Uncertain significance	Uncertain significance	14
CBS	1552T>C	Y518H				✓		✓	✓			Uncertain significance	Uncertain significance	4
TBX5	409G>A	V137M						✓	✓			Uncertain significance	Uncertain significance	7
ACTC1	710C>T	S237F				✓		✓	✓			Uncertain significance	Uncertain significance	8
PRKAG2	1366C>G	R456G						✓				Uncertain significance	Uncertain significance	13
MAP2K2	937C>T	R313W				✓		✓	✓			Uncertain significance	Uncertain significance	3

PVS1: null variant (nonsense, frameshift, canonical ± 1 or 2 splice sites, initiation codon, single or multiexon deletion) in a gene where LOF is a known mechanism of disease.

PS2: De novo (both maternity and paternity confirmed) in a patient with the disease and no family history.

PS3: Well-established *in vitro* or *in vivo* functional studies supportive of a damaging effect on the gene or gene product.

PM2: Absent from controls (or at extremely low frequency if recessive) in Exome Sequencing Project, 1000 Genomes Project, or Exome Aggregation Consortium.

PP1: Cosegregation with disease in multiple affected family members in a gene definitively known to cause the disease.

PP3: Multiple lines of computational evidence support a deleterious effect on the gene or gene product.

PP4: Patient's phenotype or family history is highly specific for a disease with a single genetic aetiology.

PP5: Reputable source recently reports variant as pathogenic, but the evidence is not available to the laboratory to perform an independent evaluation.

BS3: Well-established *in vitro* or *in vivo* functional studies show no damaging effect on protein function or splicing.

ACMG, the American College of Medical Genetics and Genomics.

in F0 fish (Supplementary material online, Figure S6). Sanger sequencing revealed various mutations in the *lmna* aCRISPR embryos (Supplementary material online, Figure S6B). The mean HR of the *lmna* aCRISPR embryos was significantly decreased compared with that of tracrRNA-injected embryos (Supplementary material online, Figure S6C and Table S3). The mean cardiac output of the *lmna* aCRISPR embryos was comparable to that of the tracrRNA-injected embryos (Supplementary material online, Figure S6D and Table S3). The mean conduction velocities of the ventricle were significantly decreased in the *lmna* aCRISPR embryos compared with that in the tracrRNA-injected embryos (Supplementary material online, Figure S6E and F and Table S3). Normalized luciferase units in the *lmna* aCRISPR embryos were comparable to those of the tracrRNA-injected embryos (Supplementary material online, Figure S7A).

We next confirmed the functional effect of PTVs (p. Q222X and p. W226X) in *EMD* using the aCRISPR method (Figure 4). We evaluated

the human *EMD* homolog using the Basic Local Alignment Search Tool. We confirmed that *emd* (ENSDART00000193281.1) in zebrafish is present in only one copy of human *EMD* and shared 45% identity with human *EMD*. The appearance and the heart morphology of both the *emd* aCRISPR and tracrRNA-injected embryos at 48 hpf was similar (Figure 4B). Sanger sequencing showed various mutations in the *emd* aCRISPR embryos (Figure 4B). The mean HR of the *emd* aCRISPR embryos was significantly decreased compared with that of the tracrRNA-injected embryos (Figure 4C and Table 5). The mean cardiac output of the *emd* aCRISPR embryos was comparable to those of the tracrRNA-injected embryos (Figure 4D and Table 5). The mean conduction velocities of the ventricle were significantly decreased in the *emd* aCRISPR embryos compared with that in the tracrRNA injected embryos (Figure 4E and F, and Table 5). Normalized luciferase units in the *emd* aCRISPR embryos were comparable to those of the tracrRNA-injected embryos (Supplementary material online, Figure S7B).

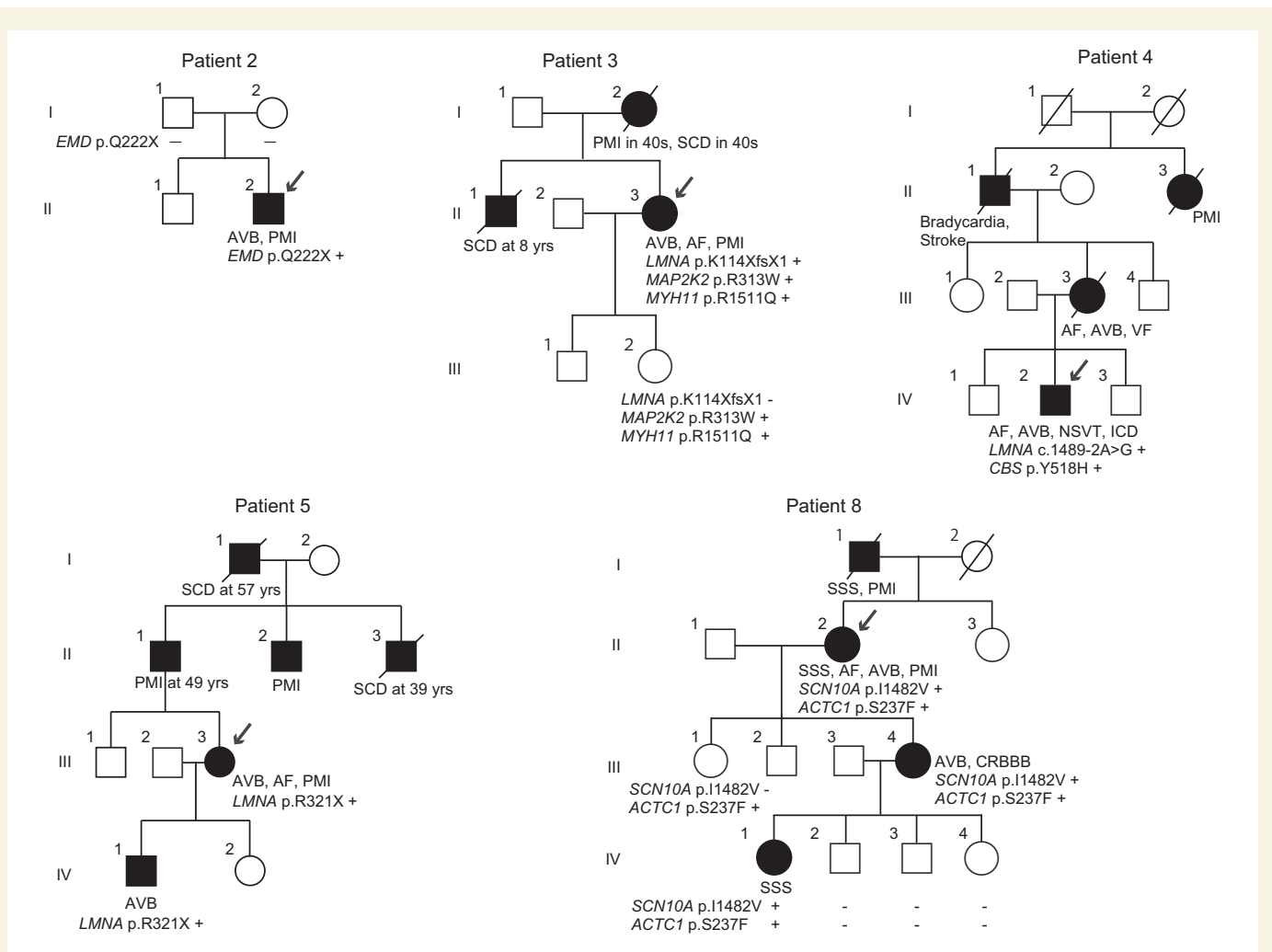


Figure 2 Pedigrees of family 2, 3, 4, 5, and 8. Squares and circles represent males and females, respectively. Slash marks represent deceased individuals. Black filled symbols indicate patients with a clinical diagnosis of CCSD. Open symbols represent unaffected family members. The probands are indicated by arrows. Plus and minus signs indicate positive and negative variants, respectively.

3.4 Clinical characteristics of a patient harbouring both rare missense variants in *KCNH2* and *SCN5A* and the functional properties of the variants by cellular electrophysiological analysis

Furthermore, we sought to define the functional effect of 2 rare missense variants classified as ‘uncertain significance’ by the guideline in *KCNH2* and *SCN5A*.

Patient 7 with *SCN5A* P1824A and *KCNH2* R269W was a 47-year-old woman.²¹ Her ECG showed SA block, AV block, and marked QT prolongation (HR 56/min, QTc 0.56 s). Holter ECG monitoring revealed a 4.5 s pause with transient loss of consciousness. She had a family history of PMI and considered to be an indication for PMI. Echocardiogram showed normal LV systolic function.

HEK293 cells were transiently transfected with vectors expressing WT or P1824A cDNA and the human beta1 subunit cDNA in combination with a bicistronic plasmid encoding GFP. Compared with the WT Nav1.5 channel, P1824A significantly reduced the peak sodium current density (Figure 5A, C and Table 6). No difference was found in persistent

sodium current between WT ($0.50 \pm 0.07\%$ of peak) and P1824A ($0.30 \pm 0.07\%$ of peak) (Figure 5B). The voltage dependence of steady-state activation of P1824A was significantly shifted in depolarizing (+5.7 mV) directions (Figure 5D and Table 6). No significant difference was observed in the voltage dependence of steady-state fast inactivation (Figure 5D).

Then, CHO-K1 cells were transiently transfected with vectors expressing WT (0.5 μ g), R269W (0.5 μ g), or WT (0.5 μ g) + R269W (0.5 μ g) in combination with the plasmid encoding GFP (Figure 5E). Electrophysiological studies showed that the maximum tail current of R269W was significantly smaller than that of WT ($P < 0.05$) (Figure 5F and Table 6). The maximum tail current of WT + R269W was comparable to that of WT alone. No significant difference in activation and deactivation kinetics was observed among three channels (Figure 5G and H, Table 6). The steady-state inactivation of R269W was significantly shifted in its voltage dependence to a negative potential compared with that of WT (Figure 5G and Table 6).

Simulation study showed that the mutational changes (by *KCNH2* R269W + *SCN5A* P1824A) in the conductance and activation/deactivation/inactivation kinetics of I_{Kr} and I_{Na} prolonged the mid-myocardial

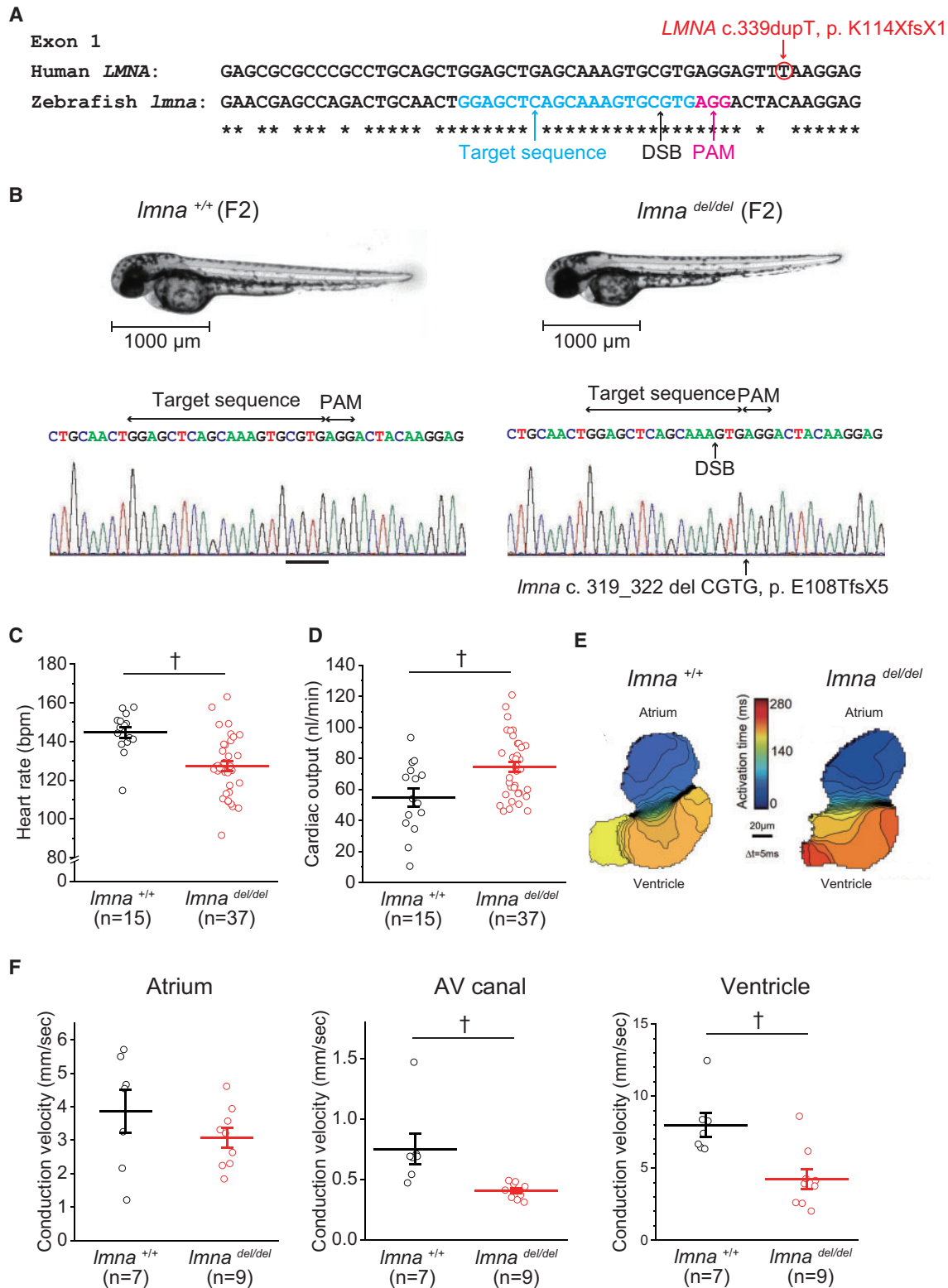


Figure 3 Functional studies of *LMNA* c.339dupT using F2 zebrafish embryos with *lmna* deletion mutation. (A) Multiple sequence alignment of human *LMNA* and zebrafish *lmna*. DSB, double-strand break; PAM, protospacer adjacent motif. (B) Representative images illustrating the morphology of 2 dpf *lmna*^{+/+} (wild-type) and *lmna*^{del/del} mutants, and Sanger sequence of *lmna* gene. (C) HR of *lmna*^{+/+} (n = 15) and *lmna*^{del/del} mutants (n = 37). (D) Cardiac output of *lmna*^{+/+} (n = 15) and *lmna*^{del/del} mutants (n = 37). (E) Isochronal map of *lmna*^{+/+} and *lmna*^{del/del} mutants summarizing the regional spread of electrical activity across the atrium and into the ventricle. The lines represent the positions of the action potential wavefront at 5-ms intervals. The colour scale depicts the timing of electrical activation (blue areas activated before red areas). (F) Mean estimated conduction velocities at the atrium, AV, atrioventricular canal, and ventricle of *lmna*^{+/+} (n = 7) and *lmna*^{del/del} mutants (n = 9). Regions of interest was placed at middle of atrium, AV canal, or ventricle. †P < 0.01.

Table 3 Summary of clinical characteristics of early-onset CCSD patients having with pathogenic or likely pathogenic variants

Patient number	Gender	Age at diagnosis (years)	SSS	AV block	FH of PMI	PMI	AF	LVEF (%)	Rare variants	Classification with PS3 (functional studies)
1	Male	33	–	✓	✓	✓	✓	53	EMD W226X	Pathogenic
2	Male	17	–	✓	–	✓	✓	60	EMD Q222X	Pathogenic
3	Female	39	✓	✓	✓	✓	✓	58	LMNA K114XfsX1 MAP2K2 R313W MYH11 R1511Q	Pathogenic
4	Male	23	✓	✓	✓	✓	✓	64	LMNA 1489-2A>G CBS Y518H	Pathogenic
5	Female	44	–	✓	✓	✓	✓	61	LMNA R321X	Pathogenic
6	Male	51	✓	–	–	✓	✓	70	SCN10A R1263X RBM20 G1217R	Likely pathogenic
7	Female	47	✓	✓	✓	✓	–	77	SCN5A P1824A KCNH2 R269W TBX5 V137M	Likely pathogenic Likely pathogenic
8	Female	42	✓	✓	✓	✓	✓	79	SCN10A I1482V ACTC1 S237F	Likely pathogenic
9	Female	31	–	✓	–	✓	–	76	SCN10A D1819Y SCN10A M1373R	Likely pathogenic
10	Male	17	✓	–	–	✓	–	60	SCN10A F507L SCN10A G805S	Likely pathogenic
11	Female	60	✓	–	✓	–	–	83	MYH7 I323T MYH6 R1116H MYH6 R1252Q	Likely pathogenic

AF atrial fibrillation; AV block, atrioventricular block; CCSD, cardiac conduction system diseases; FH, family history; LVEF, left ventricular ejection fraction; PMI, pacemaker implantation; SSS, sick sinus syndrome.

Table 4 The evaluation of cardiac function at 48 hpf and conduction velocity at 72 hpf of the F2 embryos of *lmna*^{+/+} and *lmna*^{del/del}

	<i>lmna</i> ^{+/+}	<i>lmna</i> ^{del/del}
Cardiac function	n = 15	n = 37
Heart rate (b.p.m.)	145 ± 11	127 ± 15 [†]
Stroke volume (mL)	0.39 ± 0.18	0.59 ± 0.15 [†]
Cardiac output (mL/min)	54.97 ± 22.85	74.35 ± 19.70 [†]
Fractional area change (%)	26.88 ± 8.72	38.87 ± 9.26 [†]
Conduction velocity	n = 7	n = 9
Atrium (mm/s)	3.86 ± 0.64	3.07 ± 0.30
Atrioventricular canal (mm/s)	0.75 ± 0.12	0.40 ± 0.02 [†]
Ventricle (mm/s)	7.99 ± 0.81	4.23 ± 0.68 [†]

[†]P < 0.01 vs. *lmna*^{+/+}.

action potential duration by 32% in the patient model of human ventricular myocytes paced at 1 Hz (Figure 6A-a). The normal, patient (double mutation), R269W single mutation and P1824A single mutation models exhibited early afterdepolarizations when I_{Kr} was reduced by 70%, 22%, 24%, and 69%, respectively (Figure 6A-b). The results also showed that the mutational changes slowed pacemaking in the patient peripheral SAN cell model (Figure 6B-a). Increasing GJC caused arrhythmic

dynamics (skipped beat runs) and cessation of pacemaker activity in the patient and P1824A single mutation models, but not in the normal or R269W single mutation model (Figure 6B-b).

3.5 Clinical characteristics of patients with rare PTV and missense variants in *SCN10A*, and electrophysiological studies for these variants

We found one PTV and 5 rare missense variants classified as 'uncertain significance' by the guideline in *SCN10A* in 4 of 23 patients with CCSD (Table 3). Patient 6 with *SCN10A* R1263X showed paroxysmal AF at age 49 years. He had a sinus pause of 3.6 s following termination of AF on his monitoring ECG at age 51 years, and received PMI. Patient 8 with *SCN10A* I1482V was diagnosed as SSS, AV block, and AF at age 42 years (II-2 in the Figure 2). She received PMI at the age of 56 years old. The *SCN10A* I1482V was also found in her daughter (III-4) and grandchild (IV-1) who showed AV block and SSS, respectively, and was not found in family members with a normal ECG (III-1, IV-2, 3, and 4). Patient 9 with *SCN10A* D1819Y and M1373R had AV block at age 31 years. She developed syncope at age 36 years and received PMI. Patient 10 with *SCN10A* F507L and G805S was a 17-year-old man who had SSS and received PMI. Echocardiogram of these four patients showed normal LV systolic function.

ND7/23 cells were transiently transfected with vectors expressing WT, G805S, F507L, R1263X, M1373R, I1482V, or D1819Y *SCN10A*

Table 5 The evaluation of cardiac function at 48 hpf and conduction velocity at 72 hpf of the F0 *emd* aCRISPR and *tracrRNA*- injected embryos

	<i>tracrRNA</i> -injected (control)	<i>emd</i> aCRISPR
Cardiac function	<i>n</i> = 31	<i>n</i> = 40
Heart rate (b.p.m.)	137 ± 10	121 ± 11 [†]
Stroke volume (mL)	0.61 ± 0.16	0.65 ± 0.17
Cardiac output (mL/min)	83.34 ± 21.45	79.25 ± 22.86
Fractional area change (%)	37.94 ± 7.62	37.10 ± 9.75
Conduction velocity	<i>n</i> = 7	<i>n</i> = 8
Atrium (mm/s)	6.37 ± 2.48	4.52 ± 1.99
Atrioventricular canal (mm/s)	0.86 ± 0.32	0.61 ± 0.18
Ventricle (mm/s)	19.26 ± 7.12	11.97 ± 4.58*

[†]*p* < 0.01 or **p* < 0.05 vs. *tracrRNA* injected.

cDNA in the plasmid encoding GFP. Figure 7A and Supplementary material online, Figure S8A show representative current traces recorded for these WT and rare variant Nav 1.8 channels. Neither R1263X nor M1373R generated sodium currents, whereas WT, G805S, F507L, I1482V, and D1819Y generated sodium currents. Compared with the WT, I1482V significantly increased the peak current density (Figure 7A and B, and Table 7). The voltage dependence of steady-state activation of I1482V was significantly shifted by 8.9 mV in hyperpolarizing directions (Figure 7C and Table 7). G805S variant decreased the peak sodium current density, and caused a significant depolarizing shift (+4.5 mV) in the voltage-dependence of inactivation (Figure 7D and Table 7).

3.6 Clinical characteristics of a patient with rare missense variants in *MYH6*, and functional study of one *MYH6* variant using zebrafish

Patient 11 with *MYH6* R116H and R1252Q was a 60-year-old woman who had SSS and dizziness. Her three sisters also showed bradycardia and her cousin had undergone PMI. Echocardiogram showed normal LV systolic fraction. We performed targeted *myh6* knockdown with ATG-MO. Most embryos with *myh6* MO knockdown showed a swollen pericardial sac (Supplementary material online, Figure S9A). *Myh6* morphants (*n* = 73) showed a significantly slower HR compared with non-injected embryos (*n* = 75) as described previously.¹⁷ Co-injection of *MYH6* WT (*n* = 69) or R1252Q cRNA (*n* = 70) increased HR to the extent of non-injected embryos (Supplementary material online, Figure S9B). Interestingly, cardiac oedema was rarely seen in *MYH6* WT cRNA-injected embryos compared with *MYH6* R1252Q cRNA-injected embryos (Supplementary material online, Figure S9A). The mean stroke volume and cardiac output of the *myh6* MO-injected embryos were significantly reduced compared with those of the non-injected embryos. Co-injection of *MYH6* WT RNA partially rescued the decreased mean stroke volume and cardiac output, while co-injection of *MYH6* R1252Q cRNA did not (Supplementary material online, Figure S9C and D, and Table S4). The mean conduction velocities of the ventricle were significantly decreased in the *myh6* MO-injected embryos. Co-injection of *MYH6* WT cRNA partially rescued the reduced mean conduction velocities, while co-injection of *MYH6* R1252Q cRNA did not, and showed

significantly reduced conduction velocities compared with the control (Supplementary material online, Figure S9E and Table S4).

3.7 Classification of rare variants in consideration of functional studies

Above functional studies for 13 rare variants demonstrated that 11 rare variants in *LMNA*, *EMD*, *KCNH2*, *SCN5A*, *SCN10A*, and *MYH6* could have damaging effects on each target gene (PS3), and two rare variants in *SCN10A* might not exert similar effects (BS3) (Table 2). Of those, seven variants changed their clinical significance from 'uncertain significance' to 'likely pathogenic' when added the functional study results: '1 strong (PS3) and 1 Moderate (PM2)' or '1 strong (PS3) and ≥2 supporting (PP3, PP4, and/or PP5)' (Table 2).

4. Discussion

In the present study, we analysed 23 patients with CCSD for rare variants in arrhythmia and/or cardiomyopathy-related 117 genes using HTS. Since functional studies contributed greatly to the determination of the precise pathogenicity of variants of unknown significance, we finally determined five pathogenic variants in five patients and seven likely pathogenic variants in six patients according to 2015 ACMG standards and guidelines.

This study provided some interesting findings. First, we identified two PTVs in *EMD* and three PTVs in *LMNA* as pathogenic. Also, we could confirm its pathogenicity based on functional properties of two PTVs in *LMNA* and two PTVs in *EMD* using *in vivo* zebrafish cardiac assay. This study represents the first report of the pathogenicity of PTVs in *LMNA* and *EMD* as determined by CRISPR/Cas9-mediated gene knock-out in zebrafish. *EMD* and *LMNA* are known to be the disease-causing genes of EDMD with manifestation as high-grade AV block. The former is associated with X-linked recessive inheritance and the latter with autosomal dominant, autosomal recessive, and sporadic forms of EDMD. Both genes encode nuclear envelope proteins. EDMD is a genetically heterogeneous disorder characterized by early contractures, slowly progressive muscle wasting and weakness, and cardiomyopathy with conduction block. Some patients present with conduction disturbances or atrial cardiomyopathy even when skeletal myopathy is absent and are possible candidates for these mutations. In terms of CRISPR/Cas9-mediated zebrafish analysis, it has been used as a useful *in vivo* model to assay the pathogenicity of human variants in familial cardiovascular diseases.^{22,23} Zebrafish has the advantage of transparency, low cost, and the ability to manipulate their genome efficiently. Zebrafish can gain a prominent role as the models of thousands of candidate disease-associated genes and alleles.¹⁰ Namely, human pathogenesis of CCSD with *LMNA* or *EMD* mutation could be modelled in zebrafish.

Second, we could determine the pathogenicity of six rare ion channel variants with previously defined as 'unknown significance' by two functional analyses, electrophysiological and simulation studies. *SCN5A* P1824A and *KCNH2* R269W were identified from the proband with SSS, AV block, and QT prolongation.²¹ Electrophysiological study demonstrated that both mutations showed loss-of-function. *SCN5A* encodes for the α -subunits of the voltage-gated Na⁺ channels (the Nav 1.5 channel), which is expressed in the conduction system and in the atrial regions surrounding the SAN and the AV node.²⁴ A simulation study demonstrated that *SCN5A* P1824A may contribute to sinus node dysfunction, leading to SSS because of the higher vulnerability to electrotonic modulation. In contrast, the *KCNH2* variant but not the *SCN5A*

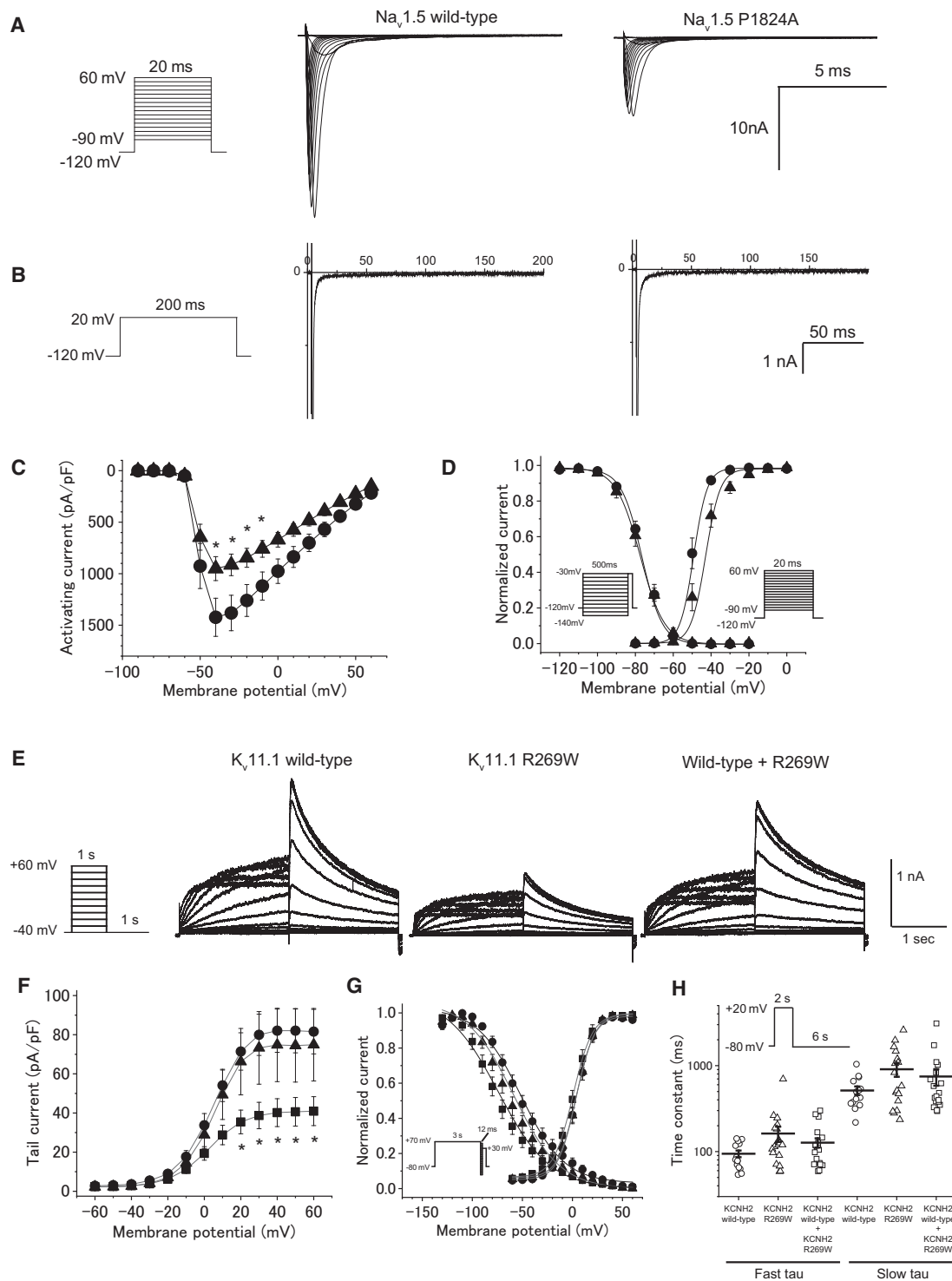


Figure 5 Functional properties of Na_v1.5 channel and K_v11.1 channel in a patient with *SCN5A* P1824A and *KCNH2* R269W. (A) The voltage protocol and representative whole-cell Na⁺ currents of the wild-type and P1824A Na_v1.5 channels. (B) Comparison of late Na⁺ currents. The late Na⁺ currents were measured at the end of 200-ms depolarizing pulses, as shown in the inset. (C) I–V relationships for peak currents in HEK293 cells transfected with wild-type (closed circle, *n* = 23) and P1824A (closed triangle, *n* = 21). **P* < 0.05 vs. wild-type. (D) The voltage protocols and the voltage dependence of steady-state fast inactivation and activation for wild-type (*n* = 19 and 23) and P1824A (*n* = 14 and 21). (E) The voltage protocol and representative expressed currents in CHO-K1 cells transfected with K_v11.1 wild-type alone, K_v11.1 R269W, and wild-type plus R269W. (F) I–V relationships for tail currents in CHO-K1 cells transfected with wild-type alone (closed circle, *n* = 19), R269W (closed square, *n* = 17), and wild-type plus R269W (closed triangle, *n* = 12). **P* < 0.05 vs. wild-type. (G) The voltage protocols and normalized steady-state activation and inactivation curves for wild-type alone (*n* = 19 and 7), R269W (*n* = 17 and 10), and wild-type plus R269W (*n* = 12 and 9). (H) The voltage protocol and fast and slow components of deactivation time constants as a function of test potentials for wild-type alone (*n* = 15), R269W (*n* = 18), and wild-type plus R269W (*n* = 20). The deactivation process was fit to biexponential functions.

Table 6 Biophysical properties of wild-type and P1824A Nav1.5 channels, and wild-type and R269W Kv11.1 channels

		Nav1.5		Kv11.1		
		Wild-type	P1824A	Wild-type	R269W	Wild-type /R269W
Cells (n)		23	21	19	17	12
Peak I_{Na} (pA/pF)		-1485 ± 186	-846 ± 131*	—	—	—
The maximum tail current (pA/pF)		—	—	84.2 ± 11.2	41.3 ± 7.4*	75.7 ± 18.7
Activation	$V_{1/2}$ (mV)	-49.5 ± 1.1	-43.8 ± 1.7*	3.8 ± 1.8	0.5 ± 2.3	3.9 ± 2.1
	SF (mV)	1.8 ± 0.2	3.4 ± 0.5*	7.9 ± 0.3	8.7 ± 0.4	8.5 ± 0.4
Cells (n)		19	14	7	10	9
Inactivation	$V_{1/2}$ (mV)	-75.9 ± 1.2	-76.6 ± 1.9	-50.1 ± 4.5	-80.8 ± 8.6*	-63.0 ± 4.8
	SF (mV)	5.1 ± 0.1	5.4 ± 0.1	20.9 ± 1.9	21.7 ± 1.7	19.7 ± 0.7
Cells (n)		—	—	17	19	21
Deactivation	$\tau_{fast, -80}$ (ms)	—	—	83.4 ± 10.6	162.3 ± 32.8	121.0 ± 16.2
	$\tau_{slow, -80}$ (ms)	—	—	514.0 ± 58.4	907.6 ± 166.2	747.0 ± 163.1

SF, Slope factor;
*P<0.05 vs. wild-type.

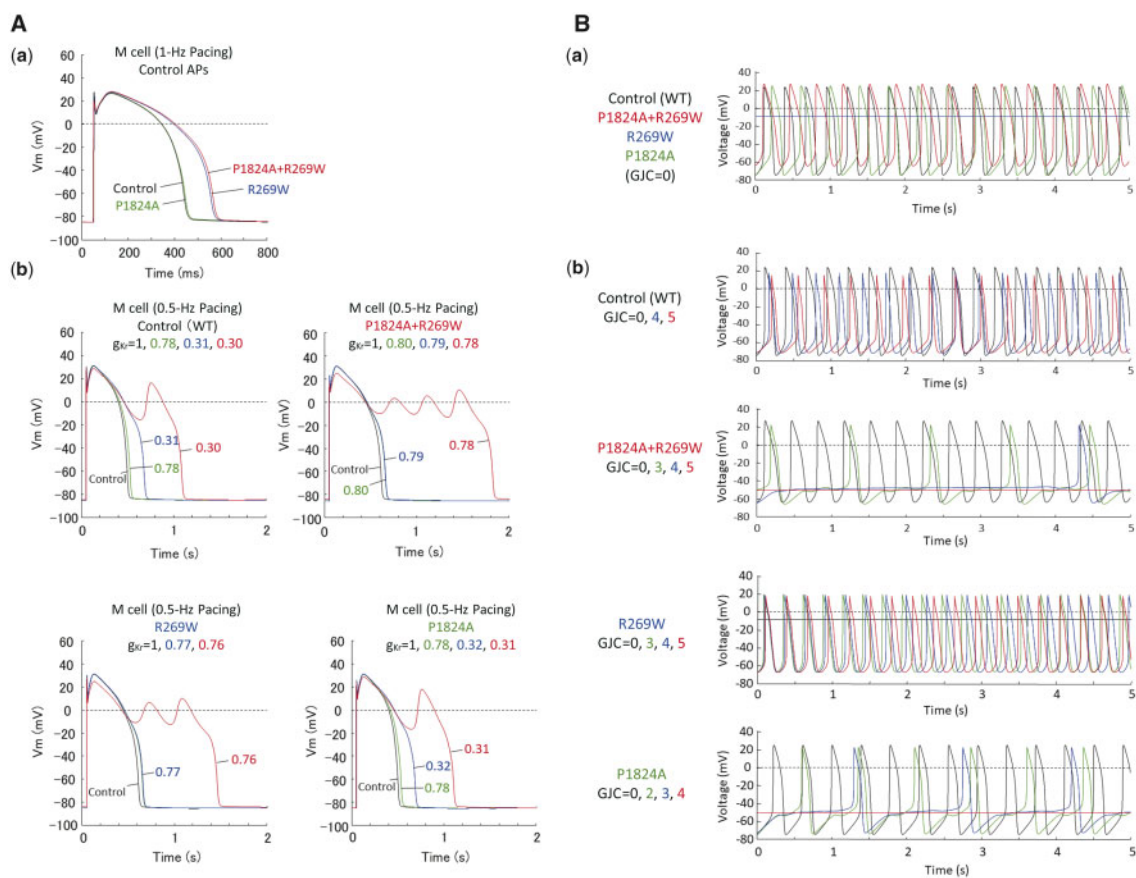


Figure 6 Computer simulation of the effects of modified kinetic behaviour of $K_v11.1$ and $Na_v1.5$ currents on electrophysiological properties of human ventricular myocytes (mid-myocardial cells) and electrotonic effects of atrial myocytes on pacemaker activity of peripheral sinoatrial node (SAN) cells in a normal subject and a patient with modified $K_v11.1$ and $Na_v1.5$ currents. (A) Simulated action potentials of ventricular mid-myocardial cell models for a normal subject and patient with modified $K_v11.1$ and $Na_v1.5$ currents (A—a). The model cells were paced at 1 Hz by 1-ms stimuli of 60 pA/pF for 30 min; steady-state behaviours after the last stimulus are shown. Modified inactivation/deactivation kinetics of R269W (*KCNH2* R269W), P1824A (*SCN5A* P1824A), and P1824A+R269W (*KCNH2* R269W and *SCN5A* P1824A) prolonged action potential duration at 90% repolarization (APD_{90}) from 400 to 517, 404, or 526 ms, respectively. Effects of I_{K_r} block on action potentials were also determined for the control and patient models, and those with *KCNH2* or *SCN5A* single mutation (A—b). (B) Simulated spontaneous action potentials in peripheral SAN cell models for the control, patient, and *KCNH2* or *SCN5A* single mutation (B—a). Action potentials were also computed for each SAN model cell connected to an atrial cell with gap junction conductance (GJC) of 0–5 nS (B—b), as described previously.²³

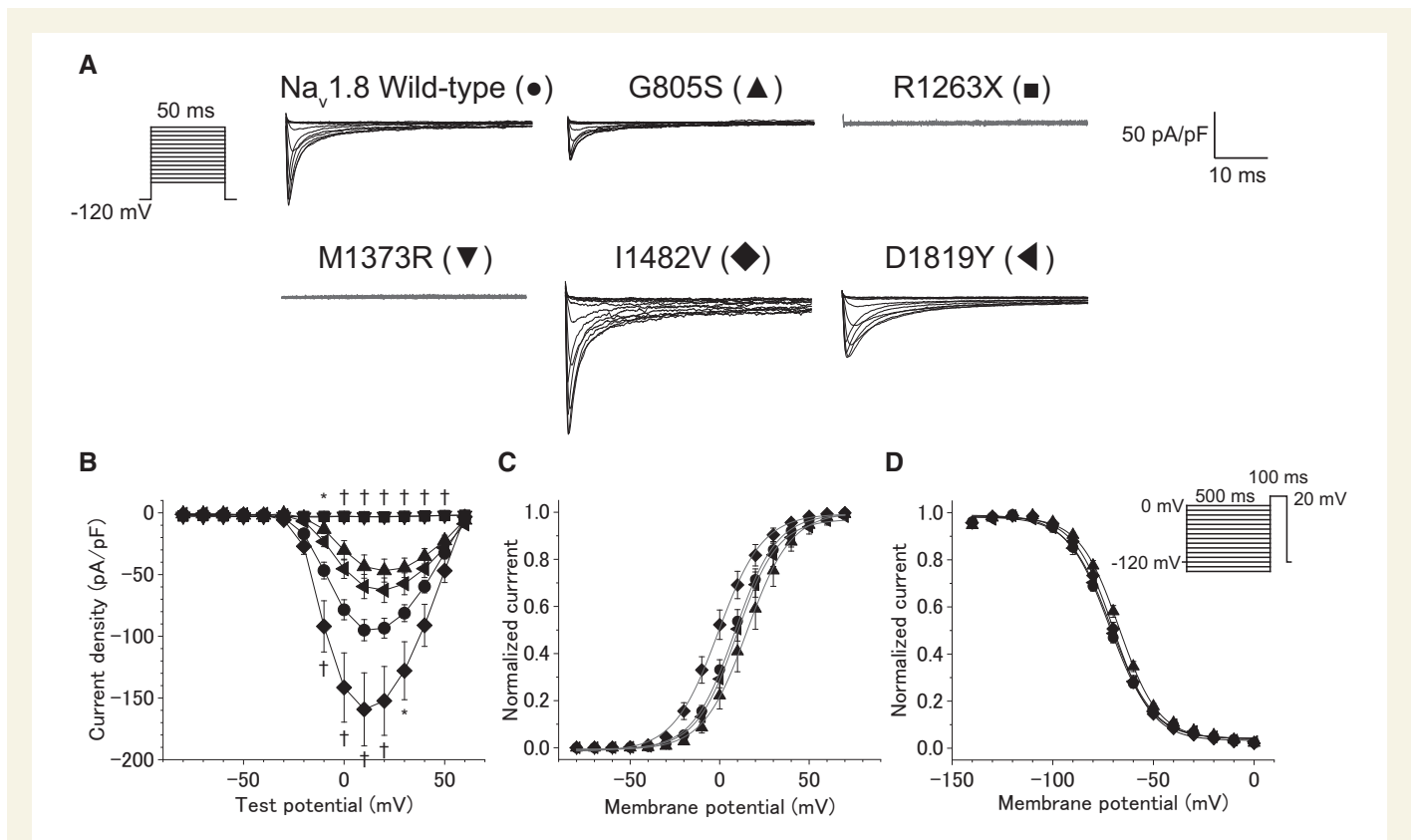


Figure 7 The functional consequence of five variants in *SCN10A* assessed by whole-cell patch clamp recording. (A) The voltage protocol and representative current traces of Na_v 1.8 using wild-type and mutant channels. (B) I-V relationships for peak currents in ND 7/23 cells transfected with *SCN10A* wild-type (●, n = 64) and five variants including G805S (▲, n = 15), R1263X (■, n = 15), M1373R (▼, n = 19), I1482V (◆, n = 25), and D1819Y (◄, n = 24). *P < 0.05 or †P < 0.01 vs. wild-type by one-way ANOVA, followed by a Bonferroni *post hoc* test. (C) Normalized steady-state activation curves of *SCN10A* wild-type (n = 64), and three variants including G805S (n = 15), I1482V (n = 25), and D1819Y (n = 24). (D) The voltage protocols and normalized steady-state inactivation curves of *SCN10A* wild-type (n = 33) and three variants including G805S (n = 13), I1482V (n = 23), and D1819Y (n = 22).

Table 7 Biophysical properties of wild-type, G805S, R1263X, M1373R, I1482V, and D1819Y Nav1.8 channels

		Wild-type	G805S	R1263X	M1373R	I1482V	D1819Y
Cells (n)		64	15	15	19	25	24
Peak I _{Na} (pA/pF)		-101.0 ± 8.9	-49.2 ± 9.5	-4.5 ± 0.4*	-4.8 ± 0.5*	-162.9 ± 30.3 [†]	-63.3 ± 9.9
Activation	V _{1/2} (mV)	9.8 ± 2.3	16.2 ± 3.8	—	—	0.9 ± 3.0*	12.2 ± 3.0
	SF (mV)	-8.9 ± 0.3	-8.7 ± 0.4	—	—	-8.2 ± 0.4	-9.6 ± 0.4
Cells (n)		33	13			23	22
Inactivation	V _{1/2} (mV)	-71.7 ± 1.0	-67.2 ± 1.1*	—	—	-70.2 ± 1.2	-71.6 ± 1.7
	SF (mV)	10.0 ± 0.3	9.6 ± 0.4	—	—	9.2 ± 0.3	9.5 ± 0.3

SF, Slope factor;

*P < 0.05 vs. wild-type;

[†]P < 0.01 vs. wild-type.

variant may contribute to QT prolongation and facilitate the formation of early afterdepolarizations during I_{Kr} inhibition, as demonstrated theoretically. Thus, the simulation study was useful in explaining the role of each variant in multiple disorders.

We determined four likely pathogenic variants in *SCN10A* in 4 of 23 (17%) CCSD patients. A cellular electrophysiological study demonstrated that three variants (G805S, R1263X, and M1373R) showed loss-

of-function effects, and one variant (I1482V) showed gain-of-function effect. The voltage-gated sodium channel alpha subunit, Nav1.8 is encoded by *SCN10A* and is highly expressed in sensory neurons of dorsal root ganglia. Several genome-wide association studies showed that *SCN10A* was associated with cardiac conduction. This is the first study to suggest that rare variants of *SCN10A* play an important role in the development of CCSD. A recent review showed how *SCN10A* variants promote

dysfunctional conduction: the cardiomyocyte, enhancer, and neuronal hypotheses.²⁵ CCSD caused by gain-of-function *SCN10A* rare variants may be explained through the neuronal hypothesis. The neuronal hypothesis stipulates that *SCN10A* indirectly exerts an effect on cardiac conduction through intracardiac neurons. *SCN10A* functions in cholinergic neurons to exert negative chronotropic and dromotropic effects on sinus and AV nodal tissues and modulates myocyte refractoriness. Gain-of-function *SCN10A* rare variants might cause vagus nerve stimulation and cardiac conduction disturbance. In contrast, the mechanism of causing CCSD by *SCN10A* loss-of-function rare variants is poorly understood. One possibility is that the enhancer hypothesis may be associated with the onset of CCSD by these variants. The enhancer hypothesis states that the cardiac enhancer located in *Scn10a* interacted with the promoter of *Scn5a* and was essential for *Scn5a* expression in murine cardiac tissue. Further studies are needed to clarify the mechanism by which loss-of-function *SCN10A* rare variants modulate cardiac conduction and lead to development of bradycardia.

This study has several limitations. First, only 117 genes linked to arrhythmogenic diseases or cardiomyopathies were examined for rare variants associated with CCSD. Causative genes may be included in the remaining genes other than these 117 genes. Second, familial aggregation and segregation analysis were inadequate. Gene analyses for family members are needed to assign the PP2 category according to the 2015 ACMG guideline. Third, approximately 30% of the human genes do not have functional homologs in zebrafish. Fourth, one of the studied two *LMNA* PTVs and one of the studied two *EMD* PTVs were not conserved in zebrafish. Furthermore, CRISPR/Cas9 cannot modify such variants. However, CRISPR/Cas9-mediated gene knock-out in zebrafish recapitulated the pathogenicity of PTVs in *LMNA* and *EMD*. In addition, functional properties of most missense variants in non-ion channel genes were not evaluated in this study. Well-established *in vitro* and *in vivo* functional studies are needed.

5. Conclusions

Integrated HTS targeting 117 arrhythmia and cardiomyopathy-related genes with functional studies identified 12 pathogenic or likely pathogenic variants in 11 of 23 CCSD probands (48%): 5 probands harbouring 5 pathogenic variants in genes encoding nuclear envelope proteins; 5 probands harbouring at least one likely pathogenic variant in genes encoding ion channels; and 1 proband harbouring one likely pathogenic variant in *MYH6*. Notably, *SCN10A* may be one of the major development factors in CCSD.

Supplementary material

Supplementary material is available at *Cardiovascular Research* online.

Authors' contributions

All authors contributed to the work described in the article and all take responsibility for it. K.H., Y.A., M.B., Y.K., I.K., C.M., S.T., and M.Y. designed the study. K.H., N.F., H.F., K.S., K.O., M.N., Y.K., T.T., B.K., K.O., Y.T., T.K., M.I., T.F., T.K., A.F., H.T., A.H., C.N., Y.S., T.T., Y.N., Y.T., H.O., Y.S., M.K., and M.T. conducted cardiovascular screening, examination, and clinical follow-up. K.H., R.T., Y.A., M.B., Y.K., E.B., P.S., M.B., Y.Z., A.K., Y.T., D.C., K.U., S.C., and T.K. performed experiments and collected the

data. K.H., A.N., R.T., Y.A., and Y.K. analysed the data. K.H., A.N., R.T., Y.A., Y.K. and M.Y. wrote the manuscript.

Acknowledgements

The authors gratefully acknowledge Takako Obayashi, and Hitomi Oikawa for technical assistance.

Conflict of interest: none declared.

Funding

This study was supported by the Grant-in-Aid for Scientific Research (C) [26460670 to K.H.] and Fund for the Promotion of Joint International Research [15KK0302 to K.H.], Takeda Science Foundation (to K.H.), SENSHIN Medical Research Foundation. (to K.H.), Suzuken Memorial Foundation (to K.H.), and Japan Heart Foundation/Bayer Yakuhin Research Grant Abroad (to R.T.).

References

1. Beinart R, Ruskin J, Milan D. The genetics of conduction disease. *Heart Fail Clin* 2010; **6**:201–214.
2. Wolf CM, Berul CI. Inherited conduction system abnormalities—one group of diseases, many genes. *J Cardiovasc Electrophysiol* 2006; **17**:446–455.
3. Ishikawa T, Tsuji Y, Makita N. Inherited bradyarrhythmia: a diverse genetic background. *J Arrhythm* 2016; **32**:352–358.
4. Celestino-Soper PB, Doytchinova A, Steiner HA, Uradu A, Lynnes TC, Groh WJ, Miller JM, Lin H, Gao H, Wang Z, Liu Y, Chen PS, Vatta M. Evaluation of the genetic basis of familial aggregation of pacemaker implantation by a large next generation sequencing panel. *PLoS One* 2015; **10**:e0143588.
5. Ho CY, Charron P, Richard P, Girolami F, Van Spaendonck-Zwarts KY, Pinto Y. Genetic advances in sarcomeric cardiomyopathies: state of the art. *Cardiovasc Res* 2015; **105**:397–408.
6. Richards S, Aziz N, Bale S, Bick D, Das S, Gastier-Foster J, Grody WW, Hegde M, Lyon E, Spector E, Voelkerding K, Rehms HL; on behalf of the ACMG Laboratory Quality Assurance Committee. Standards and guidelines for the interpretation of sequence variants: a joint consensus recommendation of the American College of Medical Genetics and Genomics and the Association for Molecular Pathology. *Genet Med* 2015; **17**:405–424.
7. Hayashi K, Konno T, Tada H, Tani S, Liu L, Fujino N, Nohara A, Hodatsu A, Tsuda T, Tanaka Y, Kawashiri MA, Ino H, Makita N, Yamagishi M. Functional characterization of rare variants implicated in susceptibility to lone atrial fibrillation. *Circ Arrhythm Electrophysiol* 2015; **8**:1095–1104.
8. Milan DJ, Macrae CA. Zebrafish genetic models for arrhythmia. *Prog Biophys Mol Biol* 2008; **98**:301–308.
9. Sabeh MK, Kekhia H, Macrae CA. Optical mapping in the developing zebrafish heart. *Pediatr Cardiol* 2012; **33**:916–922.
10. Davis EE, Frangakis S, Katsanis N. Interpreting human genetic variation with *in vivo* zebrafish assays. *Biochim Biophys Acta* 2014; **1842**:1960–1970.
11. Gagnon JA, Valen E, Thyme SB, Huang P, Ahkmetova L, Pauli A, Montague TG, Zimmerman S, Richter C, Schier AF. Efficient mutagenesis by Cas9 protein-mediated oligonucleotide insertion and large-scale assessment of single-guide RNAs. *PLoS One* 2014; **9**:e98186.
12. Liu J, Zhou Y, Qi X, Chen J, Chen W, Qiu G, Wu Z, Wu N. CRISPR/Cas9 in zebrafish: an efficient combination for human genetic diseases modeling. *Hum Genet* 2017; **136**:1–12.
13. McLaren W, Pritchard B, Rios D, Chen Y, Flicek P, Cunningham F. Deriving the consequences of genomic variants with the Ensembl API and SNP Effect Predictor. *Bioinformatics* 2010; **26**:2069–2070.
14. Panakova D, Werdich AA, Macrae CA. Wnt11 patterns a myocardial electrical gradient through regulation of the L-type Ca(2+) channel. *Nature* 2010; **466**:874–878.
15. Becker JR, Robinson TY, Sachidanandan C, Kelly AE, Coy S, Peterson RT, MacRae CA. *In vivo* natriuretic peptide reporter assay identifies chemical modifiers of hypertrophic cardiomyopathy signalling. *Cardiovasc Res* 2012; **93**:463–470.
16. Wu RS, Lam, II, Clay H, Duong DN, Deo RC, Coughlin SR. A rapid method for directed gene knockout for screening in G0 zebrafish. *Dev Cell* 2018; **46**:112–125.e4.
17. Ishikawa T, Jou CJ, Nogami A, Kowase S, Arrington CB, Barnett SM, Harrell DT, Arimura T, Tsuji Y, Kimura A, Makita N. Novel mutation in the alpha-myosin heavy

- chain gene is associated with sick sinus syndrome. *Circ Arrhythm Electrophysiol* 2015;**8**:400–408.
18. Kurata Y, Hisatome I, Matsuda H, Shibamoto T. Dynamical mechanisms of pacemaker generation in IK1-downregulated human ventricular myocytes: insights from bifurcation analyses of a mathematical model. *Biophys J* 2005;**89**:2865–2887.
 19. Kurata Y, Matsuda H, Hisatome I, Shibamoto T. Regional difference in dynamical property of sinoatrial node pacemaking: role of na⁺ channel current. *Biophys J* 2008;**95**:951–977.
 20. Sakata K, Shimizu M, Ino H, Yamaguchi M, Terai H, Fujino N, Hayashi K, Kaneda T, Inoue M, Oda Y, Fujita T, Kaku B, Kanaya H, Mabuchi H. High incidence of sudden cardiac death with conduction disturbances and atrial cardiomyopathy caused by a nonsense mutation in the STA gene. *Circulation* 2005;**111**:3352–3358.
 21. Itoh H, Shimizu W, Hayashi K, Yamagata K, Sakaguchi T, Ohno S, Makiyama T, Akao M, Ai T, Noda T, Miyazaki A, Miyamoto Y, Yamagishi M, Kamakura S, Horie M. Long QT syndrome with compound mutations is associated with a more severe phenotype: a Japanese multicenter study. *Heart Rhythm* 2010;**7**:1411–1418.
 22. Hodatsu A, Konno T, Hayashi K, Funada A, Fujita T, Nagata Y, Fujino N, Kawashiri MA, Yamagishi M. Compound heterozygosity deteriorates phenotypes of hypertrophic cardiomyopathy with founder MYBPC3 mutation: evidence from patients and zebrafish models. *Am J Physiol Heart Circ Physiol* 2014;**307**:H1594–H1604.
 23. Jou CJ, Barnett SM, Bian JT, Weng HC, Sheng X, Tristani-Firouzi M. An *in vivo* cardiac assay to determine the functional consequences of putative long QT syndrome mutations. *Circ Res* 2013;**112**:826–830.
 24. Monfredi O, Dobrzynski H, Mondal T, Boyett MR, Morris GM. The anatomy and physiology of the sinoatrial node—a contemporary review. *Pacing Clin Electrophysiol* 2010;**33**:1392–1406.
 25. Park DS, Fishman GI. Navigating through a complex landscape: SCN10A and cardiac conduction. *J Clin Invest* 2014;**124**:1460–1462.

Translational perspective

Whole-exome sequencing (WES) may be helpful in determining the causes of cardiac conduction system disease (CCSD); however, the identification of pathogenic variants remains a challenge. We performed WES of 23 probands diagnosed with early-onset CCSD, and identified 12 pathogenic or likely pathogenic variants in 11 of these probands (48%) according to the 2015 American College of Medical Genetics and Genomics (ACMG) standards and guidelines. In this context, functional analyses of a cellular electrophysiological study and *in vivo* zebrafish cardiac assay might be useful for determining the pathogenicity of rare variants, and *SCN10A* may be one of the major development factors in CCSD.